A Journal of Macroecology

Global Ecology and Biogeography

MACROECOLOGICAL METHODS

A new global burned area product for climate assessment of fire impacts

Emilio Chuvieco[1*], Chao Yue[2,3], Angelika Heil[4], Florent Mouillot[5], Itziar Alonso-Canas[1], Marc Padilla[1,6], Jose Miguel Pereira[7], Duarte Oom[7] and Kevin Tansey[6]

[1]*Environmental Remote Sensing Research Group, Department of Geology, Geography and the Environment, Universidad de Alcalá, Spain,* [2]*Laboratoire de Glaciologie et Géophysique de l'Environnement, UJF, CNRS, Saint Martin d'Hères Cedex, France,* [3]*Laboratoire des Sciences du Climat et de l'Environnement, LSCE CEA CNRS UVSQ, 91191, Gif- Sur-Yvette, France,* [4]*Max Planck Institute for Chemistry, Mainz, Germany,* [5]*UMR CEFE 5175, CNRS/Université de Montpellier/Université Paul-Valéry Montpellier/EPHE/IRD, France,* [6]*Department of Geography, University of Leicester, Leicester, UK,* [7]*Centro de Estudos Florestais, Instituto Superior de Agronomia, Universidade de Lisboa, Lisbon, Portugal*

*Correspondence: Emilio Chuvieco, Environmental Remote Sensing Research Unit, Department of Geology, Geography and the Environment, Universidad de Alcala, Colegios 2, 28801 Alcala de Henares, Spain.
E-mail: emilio.chuvieco@uah.es

ABSTRACT

Aim This paper presents a new global burned area (BA) product developed within the framework of the European Space Agency's Climate Change Initiative (CCI) programme, along with a first assessment of its potentials for atmospheric and carbon cycle modelling.

Innovation Methods are presented for generating a new global BA product, along with a comparison with existing BA products, in terms of BA extension, fire size and shapes and emissions derived from biomass burnings.

Main conclusions Three years of the global BA product were produced, accounting for a total BA of between 360 and 380 Mha year^{-1}. General omission and commission errors for BA were 0.76 and 0.64, but they decreased to 0.51 and 0.52, respectively, for sites with more than 10% BA. Intercomparison with other existing BA datasets found similar spatial and temporal trends, mainly with the BA included in the Global Fire Emissions Database (GFED4), although regional differences were found (particularly in the 2006 fires of eastern Europe). The simulated carbon emissions from biomass burning averaged 2.1 Pg C year^{-1}.

Keywords

Fire disturbance, essential climate variables, burned area, atmospheric emissions, remote sensing, MERIS, satellite earth observation, wildland fires.

INTRODUCTION

Biomass burning is one of the key components of atmospheric and terrestrial systems, as it influences emissions of various gases and aerosols, global carbon budgets and ecosystem dynamics (Krawchuk *et al.*, 2009). Naturally occurring wildfires have maintained less tree cover on some lands than there would otherwise have been and therefore they have reduced the capacity of terrestrial ecosystems to sequester carbon (Staver *et al.*, 2011; Yue *et al.*, 2015). Fires also have biophysical effects by altering the vegetation type and structure, thus changing the surface albedo and energy balance (Beck *et al.*, 2011; Rocha & Shaver, 2011). For these reasons, fire disturbance has been named by the Global Climate Observing System (GCOS) programme (GCOS 2011) as an essential climate variable (ECV). In 2010 the European Space Agency (ESA) launched a climate change initiative (CCI) programme to generate satellite-derived products that follow the specifications of GCOS (Hollmann *et al.*, 2013). The Fire_cci project is part of the CCI programme and aims to develop global information on burned area (BA) following the requirements of atmospheric and vegetation modellers (Mouillot *et al.*, 2014).

Global BA products have been developed in the past using data from various satellites/sensors (Mouillot *et al.*, 2014). The most reliable (Padilla *et al.*, 2015) are those based on the NASA's Moderate Resolution Imaging Spectrometer (MODIS) sensor, the MCD45 (Roy *et al.*, 2008) and the

DOI: 10.1111/geb.12440
http://wileyonlinelibrary.com/journal/geb

MCD64 (Giglio *et al.*, 2009). This latter BA product is one of the inputs of the Global Fire Emission Database (GFED) (v.3, Giglio *et al.*, 2010; v.4, Giglio *et al.*, 2013).

This paper presents a new global BA product, which was developed within the Fire_cci project to meet the particular requirements of the climate modelling community. The main requirements relate to spatial and temporal resolution, file formats, information on fire patch distribution and precise reporting on the uncertainty and accuracy of the final product.

Our BA dataset is the first global one based on Envisat-MERIS images. As this sensor has higher spatial resolution than MODIS BA products (300 m versus 500 m at nadir), it was hypothesized that it would have greater potential for the detection of small fires (<50 ha), which make an important contribution to global fire effects (Randerson *et al.*, 2012). This paper briefly presents the methods developed to generate the BA product, and compares this product with existing global BA datasets, both in terms of spatial and temporal trends and with regard to its potential for the estimation of fire emissions.

MATERIALS AND METHODS

Product generation

The BA algorithm combined temporal changes in near-infrared (NIR) MERIS-corrected reflectances with active fire detection from the standard MODIS thermal anomalies product, following a two-phase algorithm (Alonso-Canas & Chuvieco, 2015). Global processing of a 3-year time series (2006–08) was used to prototype the product.

Burned pixels detected by the MERIS BA algorithm were transformed to two BA products, following the recommendations of a user requirement questionnaire conducted with climate modellers.

1. The pixel product is delivered in monthly GeoTIFF files at the spatial resolution of the MERIS images (300 m at nadir, which was translated to a pixel size of 0.0029761905 geographical degrees). Files are arranged by continental tiles that make up the globe. The product includes the date when the burned pixel was first detected, a confidence level value reflecting the probability that the pixel was burned (taking into account number of detections, pre-processing assumptions and BA classification likelihood) and the land cover burned from the Globcover2005 land-cover map (Arino *et al.*, 2007). Metadata information is provided as a separate XML file.
2. The BA grid product is released in NetCDF-CF format files at 0.5° resolution covering the whole globe every 15 days. This BA product includes the total BA within each grid cell, the standard error of the BA estimation, the fraction of the observed area within each grid cell over the reporting period and the number of distinct burn patches. Furthermore, the grid product also reports BA in each grid cell for each of the 18 vegetated land-cover classes in the GLOBCover 2005 product (Arino *et al.*, 2007). The metadata are built into the NetCDF format. Further product information and downloads are available at http://www.esa-fire-cci.org/.

Validation of the final product was derived from multi-temporal pairs of Landsat images, following CEOS Cal-Val guidelines (http://lpvs.gsfc.nasa.gov/fire_home.html, last accessed November 2015). These reference data were generated for the year 2008, selecting the 105 sites from a stratified random sample (see Padilla *et al.*, 2014, 2015).

Cross-analysis with existing BA products

Spatial and temporal patterns derived from our time series (2006–08) were compared with the GFED4 BA product. GFED4 is the updated version of GFED3, which is the most widely used inventory in global biogeochemical and atmospheric modelling studies. The actual change in global BA from GFED3 to GFED4 during the period 2006–08 is only −0.1%. Some analyses were also done with GFED4s (released in July 2015). GFED4s consists of GFED4 complemented by the small fire database, following methods proposed by Randerson *et al.* (2012) based upon scaling active fire counts to BA.

To estimate emissions derived from different BA products, the ORCHIDEE dynamic global vegetation model (DGVM) (Krinner *et al.*, 2005) was used. This model was recently coupled with the prognostic fire model SPITFIRE (Yue *et al.*, 2015). Fire_cci and GFED4 BA data were originally provided with different land-cover maps (MOD12Q1 for GFED4 and Globcover2005 for Fire_cci). As DGVMs are based on the concept of plant functional types (PFTs; ORCHIDEE has 13 PFTs), BAs from observational data needed to be harmonized on a few common vegetation types. Five common vegetation types were identified: tropical forest, temperate forest, boreal forest, natural grassland and croplands. In this phase of the comparative analysis, agricultural fires were not simulated, as is common in most fire models embedded within large-scale vegetation models (except Li *et al.*, 2013). The transformation of MOD12Q1 and Globcover2005 land-cover types to the five vegetation types followed the approach of Poulter *et al.* (2011) and involved three steps: (1) assumptions were made on different PFT fractions with respect to land-cover types; (2) PFTs with the same climate types (tropical, temperate and boreal) were pooled together within the same grid cell; (3) the 13 PFTs of ORCHIDEE were further regrouped into five vegetation types.

We compared the simulated global carbon emissions and CO emissions using the ORCHIDEE model with BA being prognostically simulated, and being forced by the Fire_cci data and GFED4 data. For the prognostic simulation, the fuel combustion completeness (CC) was dynamically simulated in the model (for details see Yue *et al.*, 2014). For the simulations where observational BA data sets were used as input, the regional combustion completeness values were used (see Table 4 in van der Werf *et al.*, 2010), as constant CC (as those from GFED4 emission data set were not available). The prognostic simulation was conducted on a daily time step and the forced-BA simulations were conducted on monthly time step.

We choose fire C and CO emissions for comparison, because fire C emissions contribute to the CO_2 build-up in the atmosphere and are always used as the basis for deriving emissions for other trace gases and because CO is frequently used as a tracer of fire emissions (Leeuwen *et al.*, 2013; Poulter *et al.*, 2015). The CO emissions were derived in ORCHIDEE by using the emission factors (in units of g CO per kg dry matter consumed in fire) and C emissions ($C = 0.45 \times$ the dry mass of consumed fuel). Besides using the mean BA as reported in the Fire_cci data set, the high and low end of Fire_cci BA estimations (mean + SE and mean − SE, respectively) were also used to force the model, as a simple approach to construct the emissions uncertainty with respect to the BA uncertainty.

In addition to comparing results with existing products, new analyses focused on burn patch size and shape analysis were carried out with our Fire_cci product. Global BA analysis at the patch level has recently emerged for fire size distribution analysis based on pixel aggregation methods (Archibald *et al.*, 2010; Hantson *et al.*, 2015), helping to bridge the gap between landscape-scale and global fire regime characterization (Yue *et al.*, 2014). Most fire behaviour models embedded in DGVMs simulate elliptical burn patches. The elongation of those ellipses (the ratio between their *X*- and *Y*-axis), area and orientation are relevant for a better understanding of regional fire processes (Barros *et al.*, 2013; Mansuy *et al.*, 2014). We tested for the usability of the pixel-level product to identify individual patches within each global grid cell and generate global-scale patch metrics. We used the spatio-temporal flooding algorithm proposed by Archibald & Roy (2009) and further used in Hantson *et al.* (2015) within each $2° \times 2°$ resolution grid cell, a grid cell size in accordance with the maximum fire patch size observed world-wide (Yue *et al.*, 2014) and previously used for the global patch size distribution analysis by Hantson *et al.* (2015). We kept the largest patch computed within each grid cell and its surrounding 0.5° buffer zone, and for which the central ellipse coordinates were located within the $2° \times 2°$ grid cell. In doing so, large fires that potentially overlapped neighbouring grid cells were still considered and were referenced in the grid cell where their central coordinates belong. We cropped the continental-scale pixel product for each $2° \times 2°$ grid cell tile (plus its 0.5° buffer zone) and we re-projected it into an equal-area resolution map. Each fire patch was then characterized by several metrics: the number of cells in each patch as an indicator of fire size, the perimeter to area ratio (P/A) as an index of patch complexity, the *X*/*Y* ratio (ratio between the longest and the shortest ellipse axis defining the patch elongation) and the orientation azimuthal angle theta (angle of the fitted ellipse enveloping the fire patch: azimuthal deviation from the north of the longest axis of the ellipse). We computed these metrics for the July–August season of 2006. For comparison, a similar patch analysis was performed with fire polygons delivered by forest services at the national level for the USA (http://wfdss.usgs.gov/wfdss/), Canada (http://cwfis.cfs.nrcan.gc.ca/ha.nfdb) and Australia (Bradstock *et al.*, 2014). All analyses were performed with the R package 'raster'.

RESULTS

Product generation and validation

Figure 1 (top) shows the spatial distribution of the Fire_cci average BA for the period 2006–08. The most extensive burnings occurred in the tropical regions, particularly in the African continent, followed by the northern regions of Australia, central Brazil, Venezuelan and the Colombian Llanos and Southeast Asia. A second belt of burned regions is noticeable in the temperate grasslands and croplands of central Asia and the south-east USA. The boreal forests of Russia and Canada also have a substantial role in global biomass burnings. Total BA obtained with the MERIS algorithm ranged from 360 to 380 Mha $year^{-1}$ for the 3-year period.

The accuracy measures revealed a very high overall accuracy (99.6%), with higher errors for the burned than the unburned pixels, which is common in BA products as burned patches are much less extended globally than unburned ones. The accuracy of burned pixels was observed to be higher for areas with greater fire occurrence (omission errors decreased from 0.76 to 0.51 and commission errors from 0.64 to 0.52 in sampling sites with more than 10% BA: Alonso-Canas & Chuvieco, 2015). Comparison with existing BA products (Padilla *et al.*, 2015) showed that MERIS BA results have a similar overall accuracy to the two MODIS BA products (MCD45 and MCD64), but with higher commission and omission errors than MCD64 and higher commission error than MCD45. In terms of error balance, an overall trend towards underestimation was found (35%).

Comparison with BA products

In general, the Fire_cci product was found to be in close agreement with the GFED4 product in terms of temporal and spatial distribution (Figure 1). Mean annual BA in the Fire_cci product was 369 Mha $year^{-1}$, 6.6% higher than the estimated 346 Mha $year^{-1}$ of GFED4 (Table 1).

Absolute differences in the proportion of BA were within 5%. Larger discrepancies were confined to tropical Africa and Australia. The spatial patterns of relative differences reflected that Fire_cci tended to be notably higher in regions where small agricultural fires predominate. For example, across Europe, except for the Kazakhstan steppe region, Fire_cci estimates were two to five times higher than those from GFED4. Across agricultural India, Fire_cci estimates were typically more than four times higher than in GFED4.

In terms of land-cover classes (Fig. 2), Fire_cci exhibited the strongest contrast with GFED in woody savanna regions, where Fire_cci annual BA was higher than GFED4 by 30 Mha (or 26%). Open shrublands ranked second in terms of absolute differences; here, Fire_cci annual BA was 10 Mha (or 44%) lower than in GFED4, probably due to the

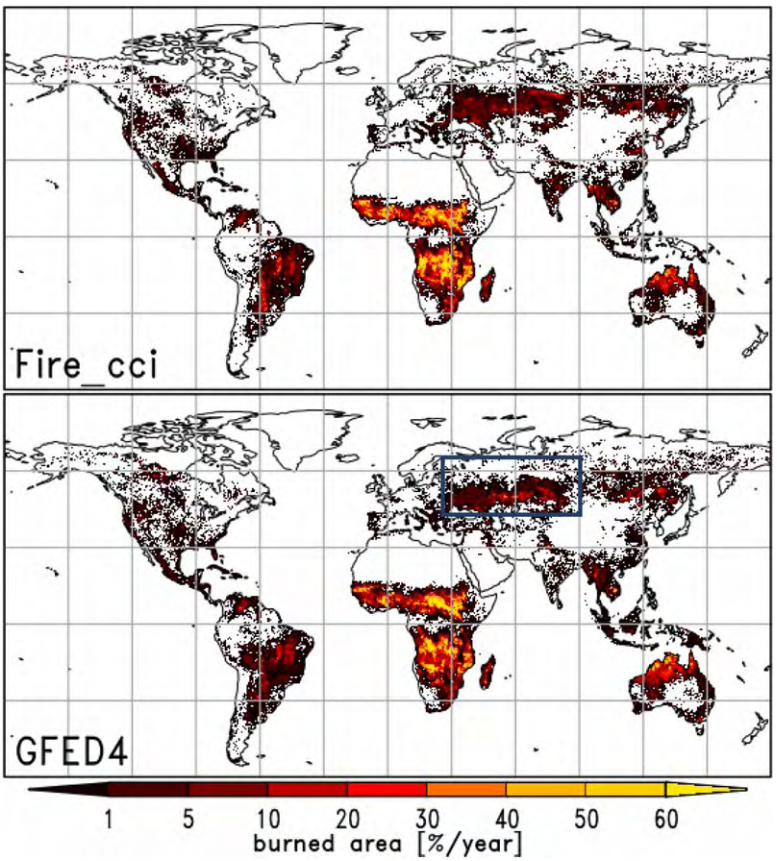

Figure 1 Mean annual proportion of burned area in each 0.5° cell for the Fire_cci and GFED4 burned area products for the period 2006–08. The box overlaying the GFED product identifies the area covered in Fig. 3.

confusion with savannas. Croplands ranked third in terms of absolute changes, with an increase in global BA of 30 Mha (or 35%). The higher spatial resolution of the MERIS sensor (300 m × 300 m compared with 500 m × 500 m in MODIS) could partially explain the higher performance of the Fire_cci product for areas with agricultural fires. Around 5.4% of all Fire_cci burned grid cells had BA sizes smaller than the lowest monthly BA in GFED4, which was 21 ha.

The global temporal patterns of Fire_cci and GFED4 BA were strongly correlated ($r^2 = 0.86$). Temporal coherence was also high on a regional scale ($r^2 > 0.5$ using the standard GFED regions, except for the boreal areas: $r^2 = 0.18$ for boreal Asia and 0.37 for boreal North America).

While Fire_cci and GFED4 showed large similarities when the products were integrated over large regions and/or temporal scales, pronounced differences emerged for specific fire events. Figure 3 shows, as an example, the differences in estimated fire-affected area during spring 2006 in eastern Europe and Central Asia. This event caused record levels of air pollution in the European Arctic, as documented by Stohl *et al.* (2007). The predominantly agricultural fires implied a strong increase in radiant energy between April and May, measured by the GFAS product which is based on detecting radiation coming from active fires using middle and thermal spectral bands (Kaiser *et al.*, 2012). While the locations of major fires were well reflected in the Fire_cci product, they were largely missed by GFED4. Yet Fire_cci shows a much lower spatial extent of the fires when compared with the recently released GFED4s database, which includes BA estimates from small fires based on active fire detections (Randerson *et al.*, 2012). This example nicely illustrates that each satellite fire product has different commission and omission characteristics dependent upon the region and the period selected.

Table 1 Estimations of global mean annual burned area, CO and carbon emissions from biomass burning for 2006–08 by different sources.

	Burned area (Mha year^{-1})	CO emissions (TgCO year^{-1})	Carbon emissions (PgC year^{-1})
GFED4 data set	346	258	1.6
ORCHIDEE-GFED4	346	329	2.0
ORCHIDEE-Prognostic	232	346	2.0
ORCHIDEE-Fire_cci	369	351	2.1
ORCHIDEE-Fire_cci HIGH	528	470	2.9
ORCHIDEE-Fire_cci LOW	206	219	1.3
GFED3.1 data set	346	334	1.9
GFED4s data set	476	339	2.1

Tg = 10^9 g, Pg = 10^{15} g.
GFED, Global Fire Emissions Database (numbers refer to different versions); ORCHIDEE, dynamic vegetation model; Fire_cci, burned area product developed within the European Space Agency's Climate Change Initiative programme.

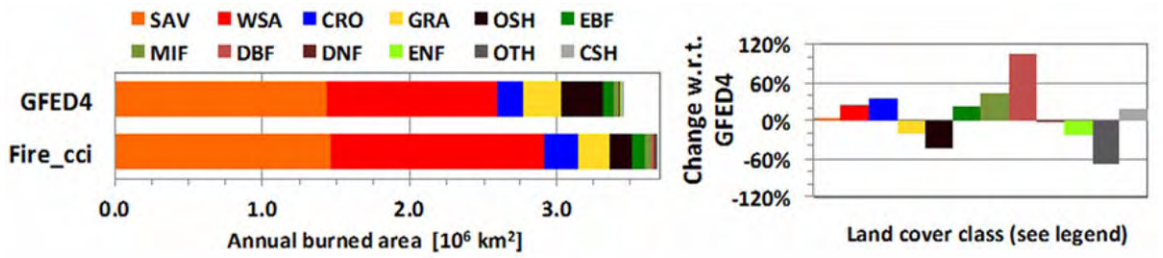

Figure 2 Annual burned area by land-cover class as estimated by Fire_cci and GFED4 (left) and relative differences between Fire_cci and GFED4 products (right). Values were computed using a 0.5° gridded map of the predominant land-cover map derived from the MODIS MCD12 v.5.1 product for the year 2005. The land-cover classes comprise: ENF, evergreen needleleaf forest; EBF, evergreen broadleaf forest; DNF, deciduous needleleaf forest; DBF, deciduous broadleaf forest; MF, mixed forest; CSH, closed shrublands; OSH, open shrublands; WSA, woody savannas; SAV, savannas; GRA, grasslands; CRO, croplands; OTH, others (merging urban and built-up areas with barren or sparsely vegetated ones).

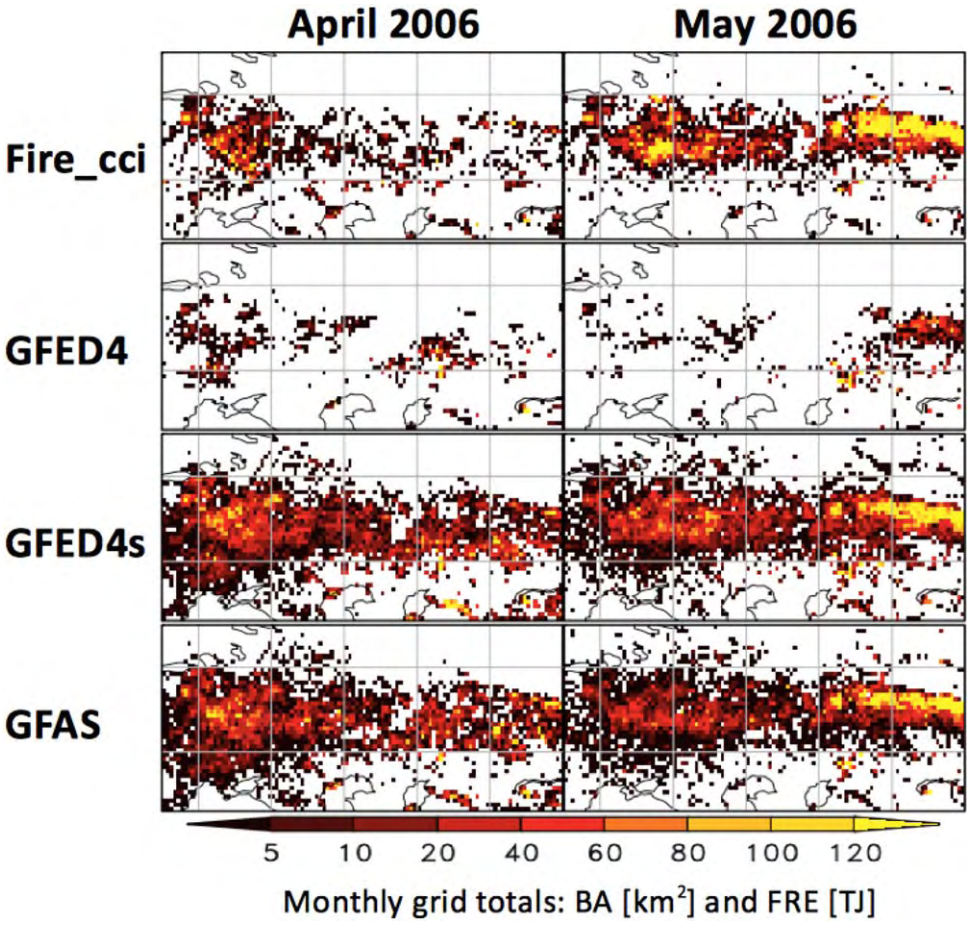

Figure 3 Burned area in eastern Europe and Central Asia detected by Fire_cci, GFED4 and GFED4s in April and May 2006. The spatial pattern of assimilated MODIS fire radiative energy (FRE) is also shown (GFAS; see Kaiser *et al.* 2012). Monthly totals per 0.5° grid for the domain 43–65° N and 25–80° E are shown. The total area burned during both months in Fire_cci, GFED4 and GFED4s, respectively, is 8.5, 1.1 and 8.4 Mha. The total radiant energy released is 71.1 TJ.

Fire patch analysis

We first used the spatial distribution of fire patch indices (for the largest fire within each 2° × 2° grid cell) across the globe to assess the coherence of pixel aggregation into patches in addition to the BA at the grid cell level for the different products. Figure 4 illustrates the global pattern of patch direction (theta, Fig. 4a), patch elongation *X*/*Y* (Fig. 4b) and patch perimeter to area ratio (P/A, Fig. 4c), and their corresponding frequency distribution according to latitudinal thresholds (45° S to 0°, 0°–45° N, 45°–90° N). Patch orientation was equally distributed according to latitude and spatially heterogeneous with no major regional pattern, indicating no major bias in the processing chain. The patch elongation index (*X*/*Y*) is normally distributed across all latitudes around a value of 1.5, with lower values for the 45° S to 0° zone indicating less elongated patches in the most fire-prone regions of tropical savannas. The regional pattern remains globally heterogeneous with contrasted values for

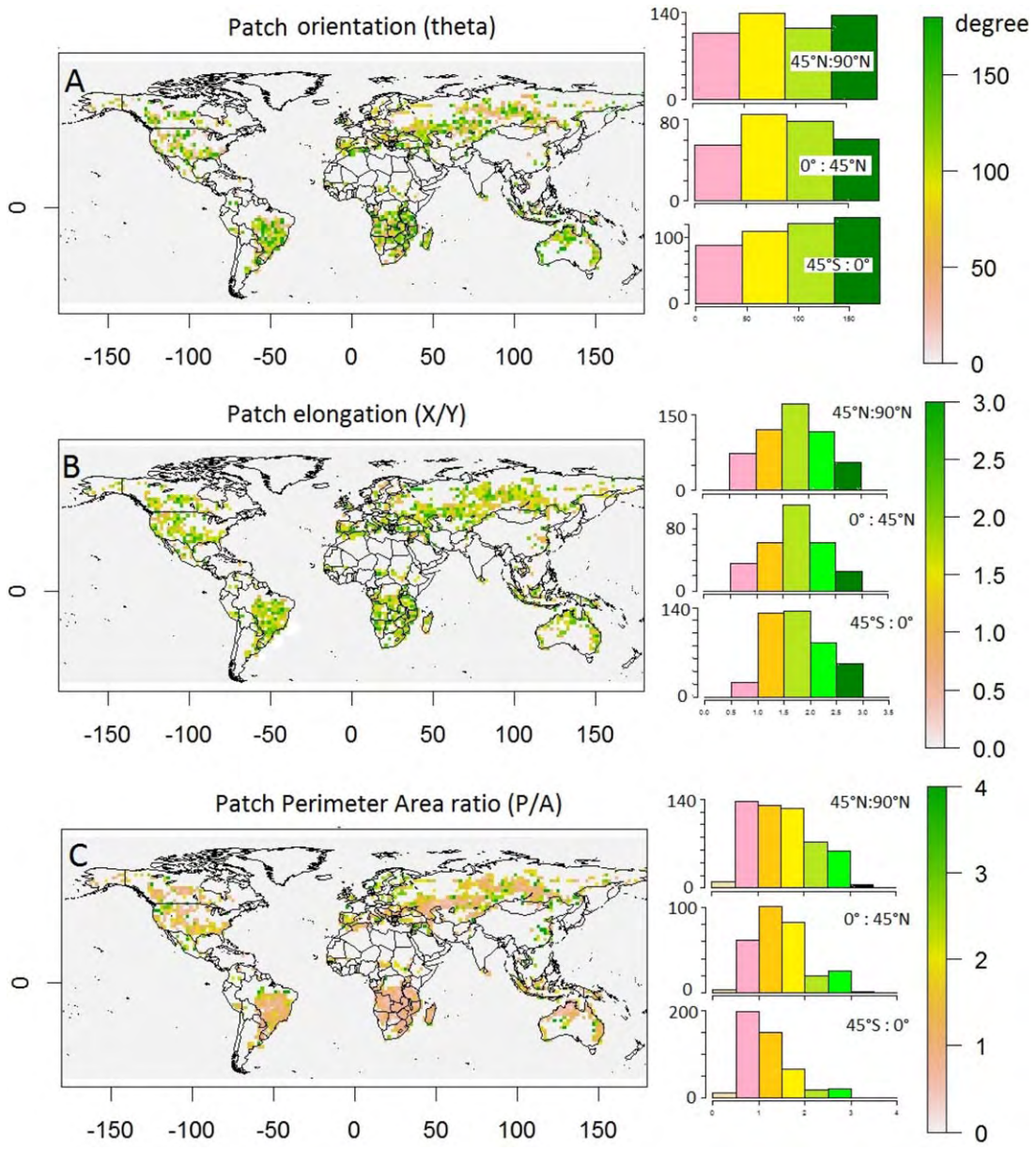

Figure 4 Global pattern of largest fire shape indices for the summer (July–August 2006) fire season (2° resolution). *X*/*Y*, patch elongation as the ratio between the longest and shortest ellipse axes ($\log_{10}$ scale); P/A, perimeter to area ratio; theta, azimuthal angle of the longest ellipse axis (degrees deviation from north).

neighbouring grid cells and a low spatial aggregation of similar fire types. The global distribution of the patch complexity index (P/A) is more related to the latitude, with a wide range of values in the northern latitudes progressively narrowing toward low values when going southward, indicating lower patch complexity when BA (and patch area) is higher.

To better assess the ability of the global pixel product to capture the actual patch structure, we compared the results obtained from fire patches derived from the BA pixel product with a similar analysis derived from fire polygons produced by national forest services in North America and Australia. Grid cell to grid cell cross-tabulations of continental maps at 2° × 2° resolution are presented in Fig. 5, for patch area thresholds of 10, 50, 100 and 200 pixels (corresponding, respectively, to 90, 450, 900 and 1800 ha), with their corresponding correlation coefficient r^2 and regression slope being given in Table 2. We observed a linear relation for patch area with $r^2 > 0.968$ for all patch size thresholds and a regression slope around 0.94 indicating a 6% underestimation of BA from MERIS compared with forest service estimates. The correlation on patch elongation (*X*/*Y*) was very low when considering all fires ($r^2 = 0.024$), but increased to 0.382 when considering fires larger than 900 ha. A similar result was observed for the patch orientation (theta), with $r^2 = 0.49$ for patch sizes >900 ha and $r^2 = 0.75$ for patch sizes >1800 ha. This

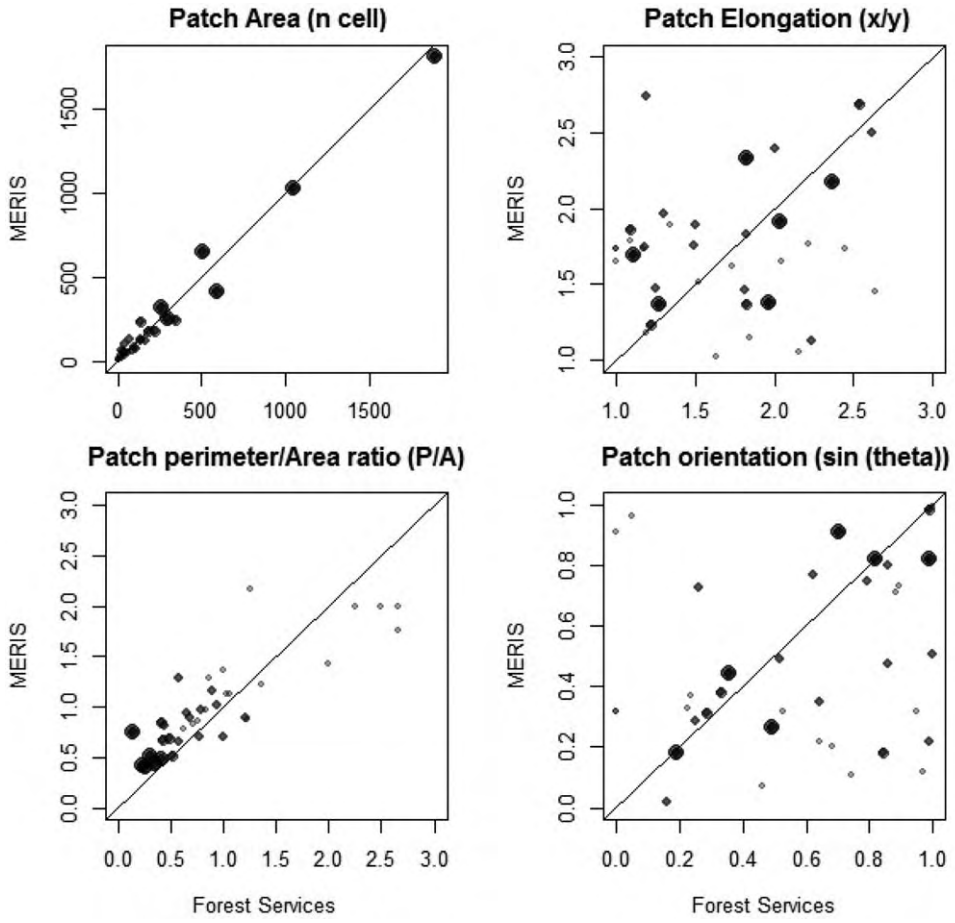

Figure 5 Relationships between patch metrics computed from the Fire_cci burned area polygons (*Y*-axis) and those derived from the forest services (*X*-axis): area (ha), elongation *X*/*Y* ($\log_{10}$), perimeter/area ratio (P/A, m m^{-2}), and orientation (theta, degrees deviation from north). The size of the circles indicates the surface of the considered fire patch, reclassified into size classes >90, >450, >900 and >1800 ha. The correlation coefficients (r^2) and slopes of the regressions are presented in Table 2.

Table 2 Correlation coefficients r^2 and regression slopes (in brackets) of the regressions between forest services fire patches and MERIS Fire_cci pixel-based fire patches. Analysis on fire size (no. of cells), patch elongation (*X*/*Y* ratio), patch complexity (perimeter/area ratio, P/A) and patch ellipse orientation (azimuthal angle theta, degrees) are presented for fire size classes >10 ha (at 1° and 2° resolution), >450 ha, >900 ha and >1800 ha. (see Fig. 5 for corresponding correlation graphs).

r^2 (slope)	Fire size	Patch elongation	Patch complexity	Patch orientation
All 1° × 1°	0.95	0.13	0.33	0.17
All 2° × 2°	0.978 (0.949)	0.024 (0.063)	0.697 (0.498)	0.057 (0.209)
2° × 2° >450 ha	0.974 (0.944)	0.101 (0.311)	0.329 (0.502)	0.249 (0.471)
2° × 2° >900 ha	0.968(0.946)	0.382 (0.570)	0.027 (0.217)	0.490 (0.727)
2° × 2° >1800 ha	0.967 (0.941)	0.254 (0.426)	0.307 (−0.772)	0.750 (0.908)

analysis illustrates the potential use of the MERIS pixel-level product for large fire shape assessment in DGVM simulations of patch elongation and direction driven by wind conditions, and as yet unexplored due to the lack of available data in global fire products. However, small fire shapes seem to remain uncertain due to the sensitivity of patch indices to burned pixel uncertainty, and the difference in fire patch resolution between global remote sensing products and local fire polygons obtained from high-resolution remote sensing or field observation. We finally obtained a low correlation between forest service polygons and MERIS P/A index for large fires ($r^2 = 0.027$ for patch sizes >900 ha), indicating a high uncertainty in patch boundaries. The correlation including all fires is much higher ($r^2 = 0.697$) as a consequence of the intrinsic strong correlation between P/A and patch size observed in the global pattern analysis.

Comparison of atmospheric emissions

BA and estimated CO and C emissions are presented in Table 1. They were based on ORCHIDEE with the prognostic simulation, and as forced by GFED4 and Fire_cci BA data, as well as on the CASA model with GFED4 BA data. As most existing fire models (Lasslop *et al.*, 2014) including ORCHIDEE are calibrated against GFED3.1 data, BA and

carbon emissions from GFED3.1 data are also provided in Table 1. Besides those values, data from the recently released GFED4s have also been included.

The annual BA estimated by the Fire_cci product was found to be similar to those obtained with the GFED3.1 and GFED4 products, but lower than the most recent estimations from GFED4s, which should be related to the consideration of small fires (Randerson *et al.*, 2012). The ORCHIDEE prognostic simulation reported a low estimate of BA (232 Mha year^{-1}), because calibrating the model gross primary productivity according to observational data (Jung *et al.*, 2011) has generally reduced the fuel load and consequently BA (see Yue *et al.*, 2015, for more details). ORCHIDEE simulations being forced by GFED4 and Fire_cci BA data, and the prognostic simulations, yielded annual fire carbon emissions of 2.0–2.1 Pg C year^{-1}, being close to those from GFED3.1 data (1.9 Pg C year^{-1}) and GFED4s data (2.1 Pg C year^{-1}). These estimations were all higher than the GFED4 data set (1.6 Pg C year^{-1}). GFED4 and GFED4s data have generally lower fire fuel consumption than GFED3.1 data, and this partly explains the higher emissions in model runs because GFED4 and GFED4s emissions have not yet been publicly released (http://www.globalfiredata.org/data.html) and all fire models are calibrated against GFED3.1 data.

The two uncertainty simulations (i.e. ORCHIDEE-Fire_cci HIGH and ORCHIDEE-Fire_cci LOW) provide the lower and higher bounds of emissions (1.3–2.9 Pg C year^{-1}), but it should be noted that a rather simple approach was used here as the heavy computation requirements of ORCHIDEE preclude a more complex uncertainty estimation approach such as Monte Carlo simulation.

The monthly carbon emission time series of fire carbon emissions are presented in Fig. 6. The correlation coefficient between the monthly carbon emission time series for the ORCHIDEE prognostic simulation and GFED4 data is 0.30, indicating that ORCHIDEE could only fairly capture the seasonality of emissions as revealed by the GFED4 data. The correlation with the GFED4 data increased to 0.65 when the model was forced by the Fire_cci BA data, and further to 0.75 when it was forced with GFED4 BA data. This showed that errors in prognostically simulating carbon emission seasonality could to a large extent be attributed to the quality of input BA data. The replacement of prognostic BA with observations improved the carbon emission simulation. The correlation between the simulations forced with Fire_cci and GFED4 was 0.92, higher than their respective correlation with the GFED4 emission data. This again confirms that Fire_cci and GFED BA data yield comparable results in fire emissions simulations.

As in the case of C emissions, prognostic and forced simulations were compared to analyse CO emissions. CO emissions forced with Fire_cci and GFED BA data gave similar estimates (329–351 Tg CO year^{-1}) to those provided by GFED3.1 and GFED4s data (334–339 Tg CO year^{-1}). The monthly time series of CO emissions resembled those of C emissions. As CO is considered as an effective tracer of fire

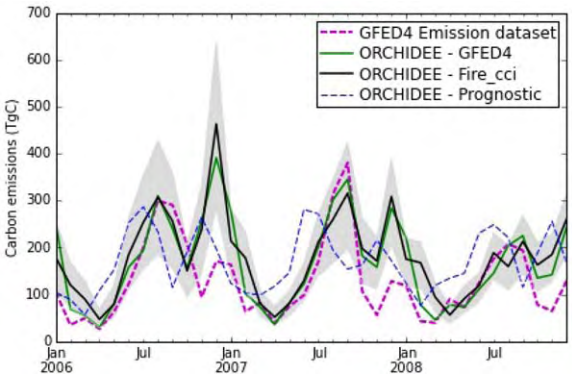

Figure 6 Monthly carbon emissions (TgC month^{-1}) from GFED4 and ORCHIDEE simulations: prognostic and forced with GFED and Fire_cci. The shaded region indicates the upper and lower bound of ORCHIDEE simulations considering Fire_cci 1 standard error uncertainty (see text).

emissions (Leeuwen *et al.*, 2013; Poulter *et al.*, 2015), we fed the fire CO emissions as reported by GFED4 and various model configurations into the atmospheric chemistry transport model LMDz-INCA and compared the agreement of resulting simulated CO mixing ratios with ground observations for 14 sites, where the CO mixing ratios are highly affected by fires (see Figure S1 in Appendix S1 in the Supporting Information for site distribution). The CO emissions from other sources and a simplified atmospheric chemistry process were included in the transport process (see Yin *et al.*, 2015, for more details). The root mean square deviation (RMSD) between de-trended monthly simulated and measured CO mixing ratio time series for 2006–08 was calculated for each site. Of the 14 sites, minimum RMSDs were reached by using ORCHIDEE-Fire_cci CO emissions data for five sites [mean RMSD by ORCHIDEE-Fire_cci is 48.7 parts per billion (p.p.b.) for these five sites], by ORCHIDEE prognostic CO emissions for seven sites (mean RMSD by ORCHIDEE is 102.2 p.p.b. for these seven sites) and by GFED4 CO emissions data for two sites (mean RMSD by GFED is 50.0 p.p.b. for these two sites) (Table S1 in Appendix S1). Despite this approach being prone to errors, in terms of atmospheric transport and chemistry processes the results show comparable performances of Fire_cci BA to GFED4 in terms of CO emissions quantification.

DISCUSSION

The Fire_cci BA product was developed as a contribution to climate modelling efforts to improve our understanding of fire dynamics in the Earth system, and the general role of fires in the climate. Being part of the GCOS programme, the requirements of climate users were recognised as a priority for the Fire_cci project. An analysis of GCOS-stated requirements (GCOS 2011) for this ECV, along with the actual demands of the climate modelling community, identified the following characteristics for an ideal BA product.

1. Long-term time series (>30 years) with a high temporal consistency (± 5%).
2. Daily temporal resolution at the original spatial resolution of the sensor (weekly, 10-day or monthly basis) on a global scale.
3. Detection of BA patches smaller than 25 ha.
4. Maximum omission and commission errors should be below 15%, with demonstrated systematic and adequate validation using internationally agreed validation protocols.
5. Error traceability and uncertainty characterization should be included in both the pixel and grid products in a manner that can be easily understood and utilized by users in various applications.
6. Easy access to data, including auxiliary information and metadata on burned cover, burn patch distribution and burn severity/efficiency.

Summarizing the main contribution of the Fire_cci BA product, we should point out that our product has made significant advances in several areas. First we were able to improve the detection of small fires by increasing the spatial resolution with respect to existing BA products (from 500 m to 300 m), which was demonstrated in the characterization of agricultural fires in eastern Europe and Central Asia. We performed the most extensive accuracy assessment done so far with global BA products (more than 300 Landsat images were used to generate the reference perimeters), using a statistically designed sample to obtain global and regional validation metrics, following standard CEOS protocols. In addition, the error and uncertainty characterization was provided at both pixel and grid level. This information was employed in a simple modelling scenario to estimate lower and upper carbon emission bounds, but additional exercises will be undertaken when longer time series are available. Finally, the Fire_cci BA product offers daily information at pixel size (date of detection) and biweekly BA totals at grid size, meeting the requirements of climate users, it includes the information layers demanded by modellers and it is easily accessible, including standard file formats and metadata.

In terms of product limitations in the framework of the GCOS requirements, the prototype Fire_cci product currently only offers a short time series (3 years), which will be extended to 15 years in the second phase of the Fire_cci project, with MERIS data complemented with other sensors. Omission and commission errors of the BA category were found to be much higher than those required by GCOS (<15%), although it should be emphasized that none of the existing global BA products meets those requirements (Padilla *et al.*, 2015). Our global BA estimations have higher errors than those of MODIS BA products, but were found to be better balanced, with less underestimation than the MODIS products (but still close to 35%). A second phase of the project will process data from higher-resolution sensors, with the target of estimating the contribution of small fires, particularly in the more fire-prone regions such as Africa.

In terms of new data analysis not previously reported at a global scale, such as the fire shape indices, the Fire_cci pixel product has been found to be very useful for describing and better understanding fire size and fire shape distributions at regional and global scales. The impacts of these spatial distributions on fire regime characterization are clear, particularly when models are available to analyse fire behaviour and fire vulnerability globally (Chuvieco *et al.*, 2014). The implications of this shape analysis on improving fire emission estimations in DGVMs has to be further evaluated, but at least it has great potential given the fact that fire size and duration in current DGVMs are poorly evaluated (Yue *et al.*, 2014).

Grid-level products derived from pixel-level analysis remain the main source of validation for coupled DGVM/fire models, but increasing the need for intermediate steps in the validation process has been pointed out by Yue *et al.* (2014). This includes fire patch size distribution and fire duration, assessed from regional datasets or regional pixel-level patch analysis (Archibald *et al.*, 2010). Fire patch information would in turn enhance model validation and improve simulations, for instance to better estimate the completeness of fuel combustion in DGVMs as larger fires are probably associated with more complete burning. On the regional level, landscape fire succession models would also benefit from fine-scale datasets as provided in the 300-m resolution Fire_cci pixel product.

From the emissions simulation analysis it can be concluded that the Fire_cci BA product can be a good complement to existing BA estimations based on MODIS data. We have demonstrated that spatial and temporal BA trends of our product are consistent with those included in GFED, but regional variations provide new insights into potential problems or strengths of existing BA databases. The extreme fires in spring 2006 in eastern Europe are an example, as the Fire_cci product appears to capture BA more realistically than GFED. Air pollution model studies including particle transport models (Evangeliou *et al.*, 2015) focusing on this event could therefore achieve better predictability with respect to measurements when using the Fire_cci product as input. Cross-comparison of multiple products is a means to validate and possibly improve individual fire products. It also helps user communities to select which product (or combination thereof) should be used for a given research question.

Finally, the climate scope of the CCI programme emphasizes the need to foster collaboration between ECV teams, which will greatly benefit both fire analysis as well as that of other ECVs. For instance, potential synergies between soil moisture, ozone, greenhouse gases or even sea temperature trends and fire occurrence and impacts have been previously suggested (Archibald *et al.*, 2013; Hantson *et al.*, 2015). The investigation of various relations among these variables, with the advantage that all the products are generated under the CCI umbrella using a consistent approach, will be undertaken within the framework of the Climate Modelling User Group (CMUG), which is also part of the CCI project.

ACKNOWLEDGEMENTS

This work was developed within the Fire Disturbance Project, in the framework of the European Space Agency Climate Change Initiative programme (grant no. 4000101779/10/I-NB). The final BA product can be freely downloaded from the web page of the Fire_cci project (http://www.esa-fire-cci.org/). Yi Yin, from LSCE provided CO simulations.

REFERENCES

Alonso-Canas, I. & Chuvieco, E. (2015) Global Burned Area Mapping from ENVISAT-MERIS data *Remote Sensing of Environment*, **163**, 140–152.

Archibald, S., Lehmann, C.E., Gómez-Dans, J.L. & Bradstock, R.A. (2013) Defining pyromes and global syndromes of fire regimes. *Proceedings of the National Academy of Sciences USA*, **110**, 6442–6447.

Archibald, S., Roy, D.P., B., V.W. & J., S.R. (2009) What limits fire? An examination of drivers of burnt area in Southern Africa. *Global Change Biology*, **15**, 613–630.

Archibald, S., Scholes, R., Roy, D., Roberts, G. & Boschetti, L. (2010) Southern African fire regimes as revealed by remote sensing. *International Journal of Wildland Fire*, **19**, 861–878.

Arino, O., Gross, D., Ranera, F., Bourg, L., Leroy, M., Bicheron, P., Latham, J., Di Gregorio, A., Brockman, C. & Witt, R. (2007) GlobCover: ESA service for global land cover from MERIS. IGARSS Symposium, pp 23–28, Barcelona.

Barros, A.M., Pereira, J., Moritz, M.A. & Stephens, S.L. (2013) Spatial characterization of wildfire orientation patterns in California. *Forests*, **4**, 197–217.

Beck, P.S., Goetz, S.J., Mack, M.C., Alexander, H.D., Jin, Y., Randerson, J.T. & Loranty, M. (2011) The impacts and implications of an intensifying fire regime on Alaskan boreal forest composition and albedo. *Global Change Biology*, **17**, 2853–2866.

Bradstock, R., Penman, T., Boer, M., Price, O. & Clarke, H. (2014) Divergent responses of fire to recent warming and drying across south-eastern Australia. *Global Change Biology*, **20**, 1412–1428.

Chuvieco, E., Martinez, S., Roman, M.V., Hantson, S. & Pettinari, L. (2014) Integration of ecological and socio-economic factors to assess global wildfire vulnerability. *Global Ecology and Biogeography*, **23**, 245–258.

Evangeliou, N., Balkanski, Y., Cozic, A., Hao, W.M., Mouillot, F., Thonicke, K., Paugam, R., Zibtsev, S., Mousseau, T.A. & Wang, R. (2015) Fire evolution in the radioactive forests of Ukraine and Belarus: future risks for the population and the environment. *Ecological Monographs*, **85**, 49–72.

GCOS. (2011) Systematic observation requirements for satellite-based products for climate, 2011 update., edn. WMO GCOS Rep. 154.

Giglio, L., Loboda, T., Roy, D.P., Quayle, B. & Justice, C.O. (2009) An active-fire based burned area mapping algorithm for the MODIS sensor. *Remote Sensing of Environment*, **113**, 408–420.

Giglio, L., Randerson, J.T., van der Werf, G.R., Kasibhatla, P.S., Collatz, G.J., Morton, D.C. & Defries, R.S. (2010) Assessing variability and long-term trends in burned area by merging multiple satellite fire products. *Biogeosciences Discuss.*, **7**, 1171–1186, doi:10.5194/bg-7-1171-2010,.

Giglio, L., Randerson, J.T. & Werf, G.R. (2013) Analysis of daily, monthly, and annual burned area using the fourth generation global fire emissions database (GFED4). *Journal of Geophysical Research: Biogeosciences*, **118**, 317–328.

Hantson, S., Pueyo, S. & Chuvieco, E. (2015) Global fire size distribution is driven by human impact and climate. *Global Ecology and Biogeography*, **24**, 77–86.

Hollmann, R., Merchant, C.J., Saunders, R.W., Downy, C., Buchwitz, M., Cazenave, A., Chuvieco, E., Defourny, P., Leeuw, G.D., Forsberg, R., Holzer-Popp, T. & Paul, F. (2013) The ESA Climate Change Initiative: satellite data records for essential climate variables. *Bulletin of the American Meteorological Society*, **94**, 1541–1552.

Jung, M., Reichstein, M., Margolis, H.A., Cescatti, A., Richardson, A.D., Arain, M.A., Arneth, A., Bernhofer, C., Bonal, D. & Chen, J. (2011) Global patterns of land-atmosphere fluxes of carbon dioxide, latent heat, and sensible heat derived from eddy covariance, satellite, and meteorological observations. *Journal of Geophysical Research: Biogeosciences (2005–2012)*, **116**.

Kaiser, J., Heil, A., Andreae, M., Benedetti, A., Chubarova, N., Jones, L., Morcrette, J.-J., Razinger, M., Schultz, M. & Suttie, M. (2012) Biomass burning emissions estimated with a global fire assimilation system based on observed fire radiative power. *Biogeosciences*, **9**, 527–554.

Krawchuk, M.A., Moritz, M.A., Parisien, M.-A., Van Dorn, J. & Hayhoe, K. (2009) Global Pyrogeography: the Current and Future Distribution of Wildfire. *PLoS ONE*, **4**, e5102.

Krinner, G., Viovy, N., De Noblet-Ducoudre, N., Ogee, J., Polcher, J., Friedlingstein, P., Ciais, P., Sitch, S. & Prentice, I.C. (2005) A dynamic global vegetation model for studies of the coupled atmosphere-biosphere system. *Global Biogeochemical Cycles*, **19**, GB1015.

Lasslop, G., Thonicke, K. & Kloster, S. (2014) SPITFIRE within the MPI Earth system model: Model development and evaluation. *Journal of Advances in Modeling Earth Systems*, **6**, 740–755.

Leeuwen, V.T., Peters, W., Krol, M. & Werf, V.D.G. (2013) Dynamic biomass burning emission factors and their impact on atmospheric CO mixing ratios. *Journal of Geophysical Research: Atmospheres*, **118**, 6797–6815.

Li, F., Levis, S. & Ward, D. (2013) Quantifying the role of fire in the Earth system–Part 1: Improved global fire modeling in the Community Earth System Model (CESM1). *Biogeosciences*, **10**, 2293–2314.

Mansuy, N., Boulanger, Y., Terrier, A., Gauthier, S., Robitaille, A. & Bergeron, Y. (2014) Spatial attributes of fire regime in eastern Canada: influences of regional landscape physiography and climate. *Landscape Ecology*, **29**, 1157–1170.

Mouillot, F., Schultz, M.G., Yue, C., Cadule, P., Tansey, K., Ciais, P. & Chuvieco, E. (2014) Ten years of global burned

area products from spaceborne remote sensing—A review: Analysis of user needs and recommendations for future developments. *International Journal of Applied Earth Observation and Geoinformation*, **26**, 64–79.

Padilla, M., Stehman, S.V. & Chuvieco, E. (2014) Validation of the 2008 MODIS-MCD45 global burned area product using stratified random sampling. *Remote Sensing of Environment*, **144**, 187–196.

Padilla, M., Stehman, S.V., Hantson, S., Oliva, P., Alonso-Canas, I., Bradley, A., Tansey, K., Mota, B., Pereira, J.M. & Chuvieco, E. (2015) Comparing the Accuracies of Remote Sensing Global Burned Area Products using Stratified Random Sampling and Estimation. *Remote Sensing of Environment*, **160**, 114–121.

Poulter, B., Cadule, P., Cheiney, A., Ciais, P., Hodson, E., Peylin, P., Plummer, S., Spessa, A., Saatchi, S. & Yue, C. (2015) Sensitivity of global terrestrial carbon cycle dynamics to variability in satellite-observed burned area. *Global Biogeochemical Cycles*, **29**, 207–222.

Poulter, B., Frank, D., Hodson, E. & Zimmermann, N. (2011) Impacts of land cover and climate data selection on understanding terrestrial carbon dynamics and the CO 2 airborne fraction. *Biogeosciences*, **8**, 2027–2036.

Randerson, J., Chen, Y., Werf, G., Rogers, B. & Morton, D. (2012) Global burned area and biomass burning emissions from small fires. *Journal of Geophysical Research: Biogeosciences (2005–2012)*, 117 - G04012, 1-23.

Rocha, A.V. & Shaver, G.R. (2011) Postfire energy exchange in arctic tundra: the importance and climatic implications of burn severity. *Global Change Biology*, **17**, 2831–2841.

Roy, D.P., Boschetti, L. & Justice, C.O. (2008) The collection 5 MODIS burned area product — Global evaluation by comparison with the MODIS active fire product. *Remote Sensing of Environment*, **112**, 3690–3707.

Staver, A.C., Archibald, S. & Levin, S.A. (2011) The Global Extent and Determinants of Savanna and Forest as Alternative Biome States. *Science*, **334**, 230–232.

Stohl, A., Berg, T., Burkhart, J., Fjæraa, A., Forster, C., Herber, A., Hov, Ø., Lunder, C., Mcmillan, W. & Oltmans, S. (2007) Arctic smoke–record high air pollution levels in the European Arctic due to agricultural fires in Eastern Europe in spring 2006. *Atmospheric Chemistry and Physics*, **7**, 511–534.

van der Werf, G.R., Randerson, J.T., Giglio, L., Collatz, G., Mu, M., Kasibhatla, P.S., Morton, D.C., Defries, R.S., Jin, Y. & Van Leeuwen, T.T. (2010) Global fire emissions and the contribution of deforestation, savanna, forest, agricultural, and peat fires (1997-2009). *Atmospheric Chemistry and Physics*, **10**, 11707–11735.

Yin, Y., Chevallier, F., Ciais, P., Broquet, G., Fortems-Cheiney, A., Pison, I. & Saunois, M. (2015) Decadal trends in global CO emissions as seen by MOPITT. *Atmospheric Chemistry and Physics Discussions*, **15**, 14505–14547.

Yue, C., Ciais, P., Cadule, P., Thonicke, K., Archibald, S., Poulter, B., Hao, W., Hantson, S., Mouillot, F. & Friedlingstein, P. (2014) Modelling the role of fires in the terrestrial carbon balance by incorporating SPITFIRE into the global vegetation model ORCHIDEE–Part 1: simulating historical global burned area and fire regimes. *Geoscientific Model Development*, **7**, 2747–2767.

Yue, C., Ciais, P., Cadule, P., Thonicke, K. & Van Leeuwen, T.T. (2015) Modelling the role of fires in the terrestrial carbon balance by incorporating SPITFIRE into the global vegetation model ORCHIDEE – Part 2: Carbon emissions and the role of fires in the global carbon balance. *Geosci. Model Dev. Discuss*, **8**, 1321–1338.

SUPPORTING INFORMATION

Additional supporting information may be found in the online version of this article at the publisher's web-site.

Appendix S1 Agreement of resulting simulated CO mixing ratios with ground observations.

BIOSKETCH

Emilio Chuvieco is currently a Professor of Geography at the University of Alcalá (Spain), where he coordinates the masters and PhD programmes in remote sensing and GIS and leads the Environmental Remote Sensing Research Group. He has coordinated 27 research projects and 20 contracts. He has supervised 35 PhD dissertations and is the co-author of 326 scientific papers and 26 books. He is the science leader of the Fire Disturbance project (Fire_cci) within the ESA Climate Change Initiative programme.

Editor: Ben Poulter